International Journal of Computational and Experimental Science and ENgineering (IJCESEN)

Vol. 11-No.4 (2025) pp. 4676-4689
http://www.ijcesen.com

ISSN: 2149-9144

Copyright © IJCESEN

Research Article

Integrated FMCW Radar Signal Processing and Image Processing for Long-Range Object Detection at 1 km

Swetha[1]*, Malateshwari Aski[2]

[1] Karnataka State AKkamahadevi Women University, Vijayapura, Karnataka
* **Corresponding Author Email:** swetha.n@kswu.ac.in - **ORCID:** 0000-0002-5247-7440

[2]Karnataka State AKkamahadevi Women University, Vijayapura, Karnataka
Email: vinnumaya25aski@gmail.com - **ORCID:** 0000-0002-5247-7050

Article Info:

DOI: 10.22399/ijcesen.5309
Received : 20 October 2025
Revised : 25 December 2025
Accepted : 28 December 2025

Keywords

FMCW radar,
long-range object detection,
Range-Doppler Map (RDM),
CA-CFAR,
image processing,
morphological enhancement

Abstract:

This paper presents an integrated FMCW radar and image-processing framework for reliable long-range object detection at distances up to 1 km. The proposed system combines 77 GHz FMCW radar signal processing with adaptive image-processing-based target enhancement to improve detection accuracy under low signal-to-noise ratio (SNR) and cluttered environments. The framework consists of four major stages: FMCW radar signal generation and channel modelling, FFT-based range–Doppler processing, CA-CFAR adaptive detection, and morphological image enhancement with blob-based target localisation. A bandwidth of 150 MHz and coherent integration over 64 chirps are employed to achieve a range resolution of 1.0 m while maintaining sufficient detection sensitivity. Simulation and analytical results demonstrate accurate target localisation with a range estimation error of only 0.5 m at a target distance of 1000 m. The obtained SNR at 1 km is approximately 38.9 dB, which is significantly above the minimum detection threshold of 13 dB. The proposed framework achieves a probability of detection of 0.9982 at a false alarm probability of 1×10^{-6}. Morphological image processing effectively suppresses isolated noise detections and enhances true target signatures in the Range-Doppler Map (RDM). Comparative analysis with existing CA-CFAR, OS-CFAR, CNN-RDM, MIMO-CFAR, and radar-camera fusion approaches demonstrates superior long-range detection capability and robustness of the proposed system. The results confirm that the proposed integrated framework provides an effective balance between long-range sensing accuracy, robustness, computational simplicity, and reliable detection performance for future automotive, surveillance, and autonomous sensing applications.

1. Introduction

Long-range object detection is an essential requirement in modern intelligent sensing systems such as autonomous vehicles, border surveillance, industrial security, unmanned aerial systems, and military monitoring applications. Detection of objects at distances close to 1 km is particularly challenging due to significant signal attenuation, clutter, adverse weather conditions, and low signal-to-noise ratio (SNR) environments [1]. High spatial resolution is offered by conventional sensing technologies such as cameras and LiDAR, but their performance degrades significantly in fog, rain, dust, smoke and low-light conditions. On the other hand, millimeter-wave (mmWave) Frequency-Modulated Continuous-Wave (FMCW) radar is robust to adverse environments and can simultaneously estimate target range and radial velocity [2].

The FMCW radar transmits the chirp signals with linear frequency modulation and extracts the target information from the beat frequency between the transmitted and received signals. The radar returns are processed using Fast Fourier Transform (FFT) based processing to obtain Range-Doppler Maps (RDMs) that contain information about the distance and velocity of targets [3],[4]. With the recent developments in CMOS and SiGe technologies, compact 77-79 GHz FMCW radar systems with high bandwidth and fine range resolution for automotive and surveillance

applications have been designed. Moreover, Multiple-Input Multiple-Output (MIMO) radar architectures improve the angular resolution by virtual aperture synthesis [5]. In spite of all the above-discussed features of stand-alone FMCW radar, there is one issue that cannot be overlooked – low reliability of object detection at large distances. The reason behind this problem is the significant reduction of received radar power at distances close to 1 km due to the nature of radar range equation [6]. Furthermore, radar reflections are subjected to influence of clutter, sidelobes, multipath effect, and thermal noise leading to false alarms generation. To mitigate these effects, adaptive thresholds, e.g., CFAR detection, can be used for clutter rejection [7]. However, the problem of remaining false alarms and low spatial resolution persists.

Simultaneously, a great number of image processing and deep learning methods, e.g., YOLO and Faster R-CNN architectures, have been developed in recent years for object detection task [8]. In spite of the achievements made, long-range object detection still represents a challenge for researchers. The main problem of this approach is that the objects at considerable distance occupy very few pixels and, therefore, are highly vulnerable to atmospheric disturbances [9]. The combination of FMCW radar signal processing and image processing techniques results in a robust detection solution that exceeds the capabilities of each sensing technique individually. The radar system provides reliable distance and speed information even under adverse weather conditions, while the imaging device provides accurate position information with complete visual and spatial details. The sensor fusion framework which combines Range-Doppler information from radar with image features shows better detection capabilities and accurate position tracking while decreasing false positiveidentifications [10]. The recent fusion methods CenterFusion and transformer-based fusion networks demonstrate effective performance for autonomous vehicles according to their results [11]. The current research mainly studies situations which occur within 300 meters, but there has been little investigation into multimodal detection methods which work at distances of 1 km [12].

The existing challenges led to the development of this integrated system which combines FMCW radar signal processing with image processing to detect objects at distances of 1 km. The proposed system unifies high-resolution FMCW radar processing with Range-Doppler analysis and adaptive CFAR detection and image-processing-based target refinement into a single perception system. The detection accuracy improves through the integration of radar and image features which help reduce false alarms and better track objects in challenging environmental conditions..

The major contributions of this work are summarized as follows:

- Development of a high-sensitivity FMCW radar processing framework for 1 km target detection.
- Integration of radar signal processing with image-processing-based small-object detection techniques.
- Design of a radar-image fusion framework for improved detection accuracy and robustness.
- Comprehensive performance evaluation using detection probability, false alarm rate, range accuracy, and processing latency metrics.

The remainder of this paper is organized as follows. Section 2 reviews related literature. Section 3 presents the system architecture and methodology. Section 4 presents results and discussion. Section 5 concludes the paper.

2. Literature review

With the rapid growth in autonomous surveillance, intelligent transportation, and defence applications, the research on integrated FMCW radar and image-processing systems for long-range object detection has seen a substantial increase. FMCW radar has been widely used as a preferred sensing technology since it can estimate the target range and velocity simultaneously in adverse environmental conditions. Li and Stoica [13] developed MIMO radar signal processing techniques and virtual array concepts that improved angular resolution without increasing the size of the antenna. Similarly, CFAR-based adaptive thresholding algorithms for the reliable detection of targets in cluttered environments were proposed by Rohling [7], which are still used extensively in modern FMCW radar systems.

The feasibility of long-range radar sensing has been improved by waveform optimisation and coherent integration techniques. Rohling and Meinecke [2] investigated the tradeoff between bandwidth, Doppler resolution and maximum detection range in FMCW systems. Later, Pfeifer et al. [14] showed that coherent integration of multiple chirps significantly improves the signal-to-noise ratio (SNR) and enables reliable target detection at ranges close to 1 km. Improvements in millimeter-wave hardware also made major

contributions to the field. Compact 77 GHz radar transceivers with high-resolution sensing for automotive and surveillance applications were presented by Hasch et al. [15].

Radar clutter suppression and target classification are still important research areas. Brennan and Reed [16] introduced space-time adaptive processing (STAP) for clutter mitigation, and Chen et al. [10] demonstrated that micro-Doppler signatures induced by human and vehicle motion can be used for target classification. Zhang et al. [17] also showed that ground-based ISAR imaging with 77 GHz FMCW radar can provide high-resolution imaging at ranges greater than 1 km, confirming the capability of millimeter-wave radar for long-range surveillance.

Deep learning applications are increasingly treating radar outputs as image-like representations. Major et al. [18] directly used convolutional neural networks (CNNs) on range-azimuth-Doppler tensors for object classification in radar, obtaining good detection accuracy for automotive applications. Gao et al. [19] extended this idea by exploiting 3D CNN architectures on range-angle-Doppler tensors for joint target localisation and classification.

Radar-camera sensor fusion also has improved considerably. Feng et al. [10] summarised multi-modal fusion architectures and claimed that feature-level fusion yields better detection results than late fusion, especially for distant objects. Nabati and Qi [11] introduced CenterFusion, a framework that fuses radar detections and camera features for better 3D object localisation. Similarly, BEVFusion proposed by Wang et al., [20] showed the effectiveness of bird's-eye-view feature representations for multi-sensor perception. However, most of the existing fusion systems are designed for short-range automotive scenarios below 100 m and are not optimised for kilometer-scale detection.

Deep learning-based small object detection has also seen considerable progress. DETR proposed by Carion et al. [8] realised the transformer-based object detection. Deformable DETR [30] improved the detection performance of small targets by the deformable attention mechanisms. Feature pyramids and attention modules are important for the detection of objects smaller than 32×32 pixels as pointed out by Cheng et al. [21], which is very relevant for 1 km imaging scenarios. For infrared imaging, DNANet was proposed by Li et al. [22] for small-target detection using dense attention mechanisms and demonstrated strong performance in thermal imagery.

However, there are significant gaps in the research. The current radar and camera fusion methods are focused on short-range autonomous driving applications. The long-range studies are mainly focused on radar processing without the use of advanced image processing and deep learning. Moreover, there are very few publicly available datasets consisting of synchronised radar and image data in the vicinity of 1 km. Thus, the aim of this work is to develop an integrated FMCW radar and image processing framework for reliable long range object detection at about 1 km using radar guided image analysis and feature level fusion techniques.

3. Methodology

The suggested approach combines FMCW radar signal processing with image processing-based detection algorithms for achieving robust detection from long distances of up to 1 km. The entire process can be divided into four successive steps: (i) simulation and generation of radar signals, (ii) processing of range-Doppler signals, (iii) enhancement and morphological processing of images, and (iv) target detection and localization. The schematic diagram of the whole process is shown in Fig. 1.

3.1 System Architecture

This detection scheme involves combining both radar and image domain processing in an effort to increase the probability of detecting the target in the low SNR scenario. In this case, initially, a radar signal is generated in a 77 GHz FMCW radar wave. After that, the returned echoes are analyzed using both one and two dimensional Fast Fourier Transformation to get the range profile and RDM. Potential target positions on the RDM are determined using the Constant False Alarm Rate (CFAR).

CFAR output is further considered as a grayscale image and subjected to processing involving adaptive thresholding as well as morphological operations so as to filter out noise components from the images as well as accentuate the target regions. This is followed by blob analysis and labeling for estimating target position and radial velocity.

3.2 Radar System Parameters

The proposed FMCW radar operates at a carrier frequency of 77 GHz with a bandwidth of 150 MHz. The radar parameters were selected to ensure sufficient range resolution and Doppler estimation capability for 1 km surveillance applications. The wavelength corresponding to the

operating frequency is approximately 3.9 mm.

The range resolution is determined by:

$$\Delta R = \frac{c}{2B} \quad (1)$$

Using a bandwidth of 150 MHz, the achieved range resolution is approximately 1 m, which is sufficient to separate closely spaced targets. The chirp duration is selected as 1 ms to avoid range ambiguity and to support coherent Doppler processing. A coherent processing interval consisting of 64 chirps is used for velocity estimation. All radar system parameters are centralized in Table 1.

3.3 W Radar Signal Model

The transmitted FMCW waveform is modeled as a linearly frequency-modulated chirp signal:

$$(t) = A_t \cos\left[2\pi\left(f_c t + \frac{1}{2} S t^2\right)\right] \quad (2)$$

where $A_t$represents the transmitted signal amplitude, $f_c$is the carrier frequency, and $S = B/T_c$denotes the chirp slope. The instantaneous frequency increases linearly over the chirp duration T_c, as illustrated in Fig. 2(a).

A target located at a distance of 1000 m introduces a round-trip propagation delay:

$$\tau = \frac{2R}{c} \quad (3)$$

The target motion additionally produces a Doppler frequency shift proportional to the radial velocity. After mixing the received signal with the transmitted chirp, a beat signal is generated whose frequency contains both range and Doppler information.

The received power is estimated using the radar range equation:

$$P_r = \frac{P_t G_t G_r \lambda^2 \sigma}{(4\pi)^3 R^4 L} \quad (4)$$

where P_t is the transmit power, G_t and G_r are the transmit and receive antenna gains, λ is the wavelength, $\sigma$is the radar cross section, and L represents system losses. For the selected system parameters and a target radar cross section of 10 dBsm, the resulting signal-to-noise ratio (SNR) is sufficient for reliable CFAR-based detection at 1 km.

The beat signal is processed using FFT-based range estimation, producing a distinct spectral peak at the true target range of 1000 m, as shown in Fig. 2(b).

3.4 Range and Doppler Processing

The first stage of signal processing performs an N-point FFT on each received chirp to convert the beat frequency into range bins. Prior to FFT computation, a Hann window is applied to reduce spectral leakage and sidelobe effects. The resulting range spectrum contains a dominant peak corresponding to the target position.

To estimate target velocity, Doppler processing is performed across multiple chirps using a second FFT along the slow-time dimension. This generates a two-dimensional Range–Doppler Map (RDM), where target reflections appear as localized high-energy peaks. The velocity resolution is given by:

$$\Delta v = \frac{\lambda}{2MT_c} \quad (5)$$

The generated RDM provides simultaneous estimation of target range and radial velocity.

3.5 CFAR-Based Target Detection

A Cell-Averaging Constant False Alarm Rate (CA-CFAR) detector is employed to identify target cells in the RDM while maintaining a constant probability of false alarm. For each Cell

Under Test (CUT), surrounding training cells are used to estimate the local noise power level. Guard cells are inserted around the CUT to prevent target energy leakage into the noise estimate.

The adaptive threshold is computed as:

$$[k, m] = \alpha[k, m] \quad (6)$$

where $Z[k, m]$ is the estimated local noise power and α is the scaling factor determined by the desired false alarm probability. A detection is declared whenever the CUT magnitude exceeds the adaptive threshold.

3.6 Image Processing and Morphological Enhancement

The binary CFAR output is processed in a similar way to an image using image processing techniques. The first step is to use Otsus adaptive thresholding to better separate the target region from the background. Morphological dilation with a 3 x 3 structuring element is then applied to connect broken target responses between neighbouring range-Doppler bins.

Then morphological erosion removes isolated noise pixels and reduces false detections . This combination of dilation and erosion enhances the continuity of real target signatures and greatly suppresses the random noise artefacts.

3.7 Blob Detection and Target Localization

Following morphological operations, connected component labeling is performed to recognize contiguous target blobs. Each identified blob is defined by its centroid, area, and bounding-box sizes. Blobs with area below the predetermined threshold value are ignored as false positives. The range and velocity of each target are then computed based on the coordinates of the detected blobs' centroids using the calibrated values for the bin sizes of the range and Doppler axes. The centroid localization technique developed offers sub-bin resolution estimates.

The outputs of the system include the indication of target existence, its estimated range, radial velocity, and corresponding detection map based on the integrated results of the radar and image processing systems.

Algorithm 1: Proposed Integrated FMCW Radar and Image Processing Framework for Long-Range Object Detection

Input: Radar parameters $(f_c, B, T_c, F_s, M, P_t, G_t, G_r, NF)$; Target parameters (R_0, v, σ); CFAR parameters (N_r, N_c, P_{FA})

Output: Detected target set $\Omega = \{(\hat{R}_i, \hat{v}_i)\}$

Stage 1: FMCW Radar Signal Generation and Channel Modeling

1. Compute radar parameters: $\lambda = \frac{c}{f_c}$, $S = \frac{B}{T_c}$, $N = F_s T_c$
2. Generate fast-time vector $t = \text{linspace}(0, T_c, N)$
3. Generate transmitted FMCW chirp: $s_t(t) = A_t e^{j(2\pi f_c t + \frac{1}{2}\mu t^2)}$
4. Compute target delay and Doppler shift: $\tau = \frac{2R_0}{c}$, $f_D = \frac{2\pi f_c}{c}$
5. Generate received signal: $s_r(t) = \frac{\sqrt{P_t}}{\sqrt{P_s}} s_t(t - \tau)e^{j(2\pi f_c t - \tau)}$
6. Add complex Gaussian noise: $s_r(t) = s_r(t) + n(t)$

Stage 2: Signal Processing and CFAR Detection

7. Generate beat signal through deramping: $x(t) = s_r(t) \cdot s_t^*(t)$
8. Apply Hann window along fast-time samples
9. Perform Range FFT: $X_r = \text{FFT}(x(t))$
10. Apply slow-time window across chirps
11. Perform Doppler FFT to obtain Range-Doppler Map (RDM): $RDM = \text{FFT}(X_r)$
12. Compute CFAR scaling factor: $\alpha = N_c (P_{FA}^{-1/N_c} - 1)$
13. Estimate local noise power from training cells: (Z[k,m]=diac{1}{N_c}sum
14. Apply CA-CFAR decision rule: $D[k, m] = 1$if (

Stage 3: Image Processing and Blob Refinement

15. Apply Otsu adaptive thresholding to CFAR output
16. Perform binary morphological dilation using a 3 × 3structuring element
17. Apply morphological opening to suppress isolated noise pixels
18. Perform connected-component labeling with 8-connectivity
19. Retain blobs satisfying $\text{Area}(\Omega_i) \geq A_{min}$

Stage 4: Target Localization and Output

20. Estimate target range and velocity for each retained blob: $\hat{R}_i = k_i \frac{\sqrt{2}c}{2B}$, $\hat{v}_i = m_i \frac{\lambda}{2MT_c}$
21. Return final detected target set $\Omega = \{(\hat{R}_i, \hat{v}_i)\}$

4 Experimental and Simulation Results

4.1 Signal Generation and Chirp Characterisation

A linear frequency modulation model with a bandwidth of 150 MHz and a chirp duration of 1 ms was used to generate the FMCW radar chirp signal. Figure 3(a) shows the instantaneous frequency variation of the transmitted chirp, where the frequency increases linearly with time, producing a chirp slope of S=150 GHz/s. The figure confirms the correct implementation of the FMCW waveform required for long-range radar sensing. Figure 3(b) shows the variation of signal-to-noise ratio (SNR) with target range due to propagation loss. At the design range of 1000 m, the obtained SNR is approximately 38.9 dB, which is well above the detection threshold of 13 dB. The figure verifies that the FMCW waveform needed for long-range radar detecting is implemented correctly. Based on the radar range equation and coherent processing gain, Figure 3(b) shows how the signal-to-noise ratio (SNR) varies with target range. As anticipated, propagation loss causes the SNR to progressively decline as range increases. The observed SNR at the 1000 m design range is around 38.9 dB, which is still far over the 13 dB detection threshold. Therefore, the figure verifies that the suggested radar arrangement has enough detection margin for accurate long-range target identification at a distance of one kilometre.

4.2 Range Processing and Beat Signal Analysis

Figure 4 shows the beat signal and the FFT-based range estimation results from the proposed FMCW radar processing chain. The complex beat signal generated after mixing the transmitted and received chirp signals is shown in Fig. 4(b). The real and imaginary parts exhibit oscillatory behaviour at the target-induced beat frequency of 1 MHz, which carries the range information of the detected object. Figure 4(a) shows the normalized FFT-based range profile after applying a Hann window and doing the fast-time FFT. A dominant spectral peak can be clearly seen near the true target position of 1000 m. The estimated target range is about 999.5 m, which is very close to the actual target distance, so the estimation error is very small, 0.5 m. The effectiveness of the FFT based range processing in accurately detecting long-range targets under noisy conditions is illustrated by the low sidelobe levels and sharp target peak.

4.3 Range-Doppler Map Generation

The 2D Range-Doppler Map (RDM) was created by Doppler FFT on the slow-time chirp dimension after range FFT processing. Figure 5 (a) shows the normalised RDM in dB, where a clear high-energy target response is observed around the range of

1000 m. The target peak is clearly separated from the background noise, confirming successful range-Doppler processing and coherent integration over multiple chirps. The power distribution is still concentrated around the target location, showing the ability of the proposed FMCW radar system to detect long-range objects with high accuracy. Figure 5(b) shows the range profile extracted at the target Doppler bin. There is a clear peak close to the true target range of 1000 m (reference dashed line). The response obtained confirms the consistency of the range FFT and Doppler FFT stages and also confirms the accurate localisation of the target in the range-Doppler domain.

4.4 CA-CFAR Detection

The Cell-Averaging Constant False Alarm Rate (CA-CFAR) detector was applied to the Range-Doppler Map (RDM) to identify potential target locations while suppressing noise and unwanted clutter. Figure 6(a) presents the normalized RDM power distribution, where the target response is concentrated near the range of 1000 m. Figure 6(b) shows the corresponding binary CA-CFAR detection map generated using a false alarm probability of P_{FA} = $10^{-6}$and a threshold scaling factor of α = 19.91. The detected target cells are clearly separated from the background noise, confirming the effectiveness of the adaptive thresholding mechanism.

Figure 6(c) illustrates the range cut at the target Doppler bin together with the adaptive CFAR threshold. The signal power exceeds the threshold near the true target position at 1000 m, indicated by the dashed reference line, resulting in successful target detection. The adaptive threshold closely follows the surrounding noise floor, demonstrating that the CA-CFAR algorithm effectively maintains reliable detection performance while minimizing false alarms under noisy conditions.

4.5 Image Processing and Morphological Enhancement

Following CFAR detection, the binary detection map is processed as a grayscale image using morphological operations. Figure 7 illustrates the four-stage image processing pipeline. Stage (a) shows the raw CFAR binary output with 10 detections. Stage (b) demonstrates the effect of Otsu adaptive re-thresholding followed by binary dilation with a 3×3 structuring element, which connects fragmented target responses across adjacent range-Doppler bins. Stage (c) shows the result after morphological opening (erosion applied to the dilated map), which removes isolated noise pixels while preserving true target blobs. Stage (d) presents the final detection map after connected-component labelling and area filtering. The image processing step provides a large noise suppression, confirming the effectiveness of the morphological operations to reduce the false alarms while keeping the detection of the true target signature.

4.6 System Performance Characterisation

Figure 8 presents the key performance characterisation results of the proposed radar detection system. Figure 8(a) illustrates the variation of signal-to-noise ratio (SNR) with target range, calculated using the radar range equation including coherent processing gain. The obtained SNR at a target distance of 1 km is 38.89 dB, which exceeds the minimum detection threshold of 13 dB by approximately 25.9 dB, indicating robust detection capability under the considered operating conditions. The analysis further shows that the theoretical maximum detection range corresponding to the threshold SNR is approximately 1.6 km. Figure 8(b) presents the theoretical probability of detection (P_d) versus SNR for a Swerling Case I fluctuating target model using CA-CFAR with a false alarm probability of P_{fa} =1 × 10^{-6}. At the operating SNR of 38.89 dB, the system achieves a detection probability of approximately 0.9982, demonstrating highly reliable target detection performance. Figure 8(c) illustrates the CA-CFAR sliding window configuration employed in the proposed framework, showing the Cell Under Test (CUT), guard cells, and training cells used for adaptive threshold estimation. The configuration uses N_g = 3guard cells and N_t = 10training cells on each side of the CUT to balance accurate noise estimation and target protection.

4.7 Monte Carlo Validation

To validate the theoretical performance model, a Monte Carlo simulation was conducted with N_MC = 500 independent trials per SNR operating point. Each trial generated a fresh noise realisation, applied a Hann-windowed range FFT, and evaluated the CA-CFAR decision rule for the target cell. Figure 9 compares the empirically measured Pd with the theoretical Swerling Case I prediction across a range of SNR values from 0 to 25 dB. The empirical results fit well with the theoretical curve, in particular for SNR above 15 dB, where detection is very reliable. Small deviations from the theoretical curve at low SNR values are expected due to the finite Monte Carlo

sample size. The design operating point (SNR= 38.89 dB) lies well to the right of the region where Pd approaches unity, further confirming the robustness of the proposed system design.

4.8 Bandwidth–Resolution Trade-off Analysis

Figure 10 and Table 2 show the effect of bandwidth variation on range resolution and SNR performance of the proposed FMCW radar system. As can be seen in Fig. 10(a), the range resolution becomes significantly better for increasing bandwidth, decreasing from 3.0 m at 50 MHz to 0.15 m at 1 GHz following the inverse proportionality $\Delta R=c/(2B)$. This demonstrates the advantage of larger bandwidths, in terms of finer target separation and better localisation accuracy.

The corresponding SNR variation at the design range of 1 km is shown in Figure 10(b). Increasing the bandwidth improves the range resolution but also increases the receiver noise bandwidth, thus leading to a slow decrease in SNR. The SNR drops from 24.9 dB at 50 MHz to 11.9 dB at 1 GHz. At very high bandwidths , the SNR approaches and eventually drops below the minimum detection threshold of 13 dB , leading to degraded detection reliability . The chosen operating bandwidth of 150 MHz provides a good compromise between resolution and detection performance. With this bandwidth the system obtains a range resolution of 1.0 m while maintaining an SNR of 20.1 dB at 1 km, which is still well above the required detection threshold. These results confirm that the bandwidth chosen is suitable for reliable long-range FMCW radar detection.

4.9 Comparative Performance Summary

Table 3 compares the performance of the proposed integrated FMCW radar and image-processing framework with several representative radar detection approaches reported in the literature. The comparison includes conventional CFAR-based techniques, MIMO radar processing, deep learning–based Range-Doppler classification methods, and radar-camera fusion approaches operating in the 77 GHz automotive radar band.

The proposed system demonstrates superior long-range detection capability, achieving reliable target detection beyond 1 km while maintaining a probability of detection (P_d) of 0.998 at a false alarm probability of P_{fa} = 10^{-6}. In comparison, conventional CA-CFAR and OS-CFAR methods provide acceptable detection performance but are generally limited to ranges below 800 m due to reduced robustness in noisy and cluttered environments. Deep learning–based CNN-RDM approaches achieve improved classification accuracy; however, their reported detection ranges are typically restricted to short-range scenarios of approximately 70 m. The MIMO-CFAR approach provides finer range resolution of 0.5 m through spatial diversity and virtual array processing, but its operational detection range remains lower than that achieved by the proposed framework. Similarly, radar-camera fusion methods offer enhanced environmental perception and object classification capabilities; however, their effectiveness is constrained by camera visibility and short-to-medium range operation, typically below 300 m. The superior performance of the proposed framework is primarily attributed to the integration of adaptive CA-CFAR processing with morphological image enhancement and blob-based target localization. This combined radar–image processing strategy significantly suppresses false alarms while preserving coherent target responses, enabling highly reliable long-range detection performance without requiring computationally intensive deep learning architectures. Overall, the results confirm that the proposed method provides an effective balance between detection accuracy, range capability, computational simplicity, and robustness for long-range FMCW radar applications.

4.10 Discussion

The obtained simulation and analytical results demonstrate that the proposed integrated framework of FMCW radar and image processing can provide reliable long-range target detection with high accuracy and robustness. The generated FMCW chirp signal exhibited the expected linear frequency modulation features with a chirp slope of 150 GHz/s, confirming the correct implementation of the waveform generation stage. The SNR analysis shows that the system can work with an SNR of about 38.9 dB at a design range of 1000 m, i.e., much higher than the minimum detection threshold of 13 dB. This large detection margin proves the appropriateness of the proposed radar configuration for kilometre scale sensing applications. The range processing stage using FFT detected the target correctly at about 999.5m, which translates into a very small range estimation error of only 0.5m. The sharp spectral peak and low sidelobe behaviour in the range profile confirm the effectiveness of the Hann-windowed FFT processing for accurate long range target localisation under noisy conditions. The generated Range-Doppler Map (RDM) also showed a good separation between the target response and background noise, which proves the efficient

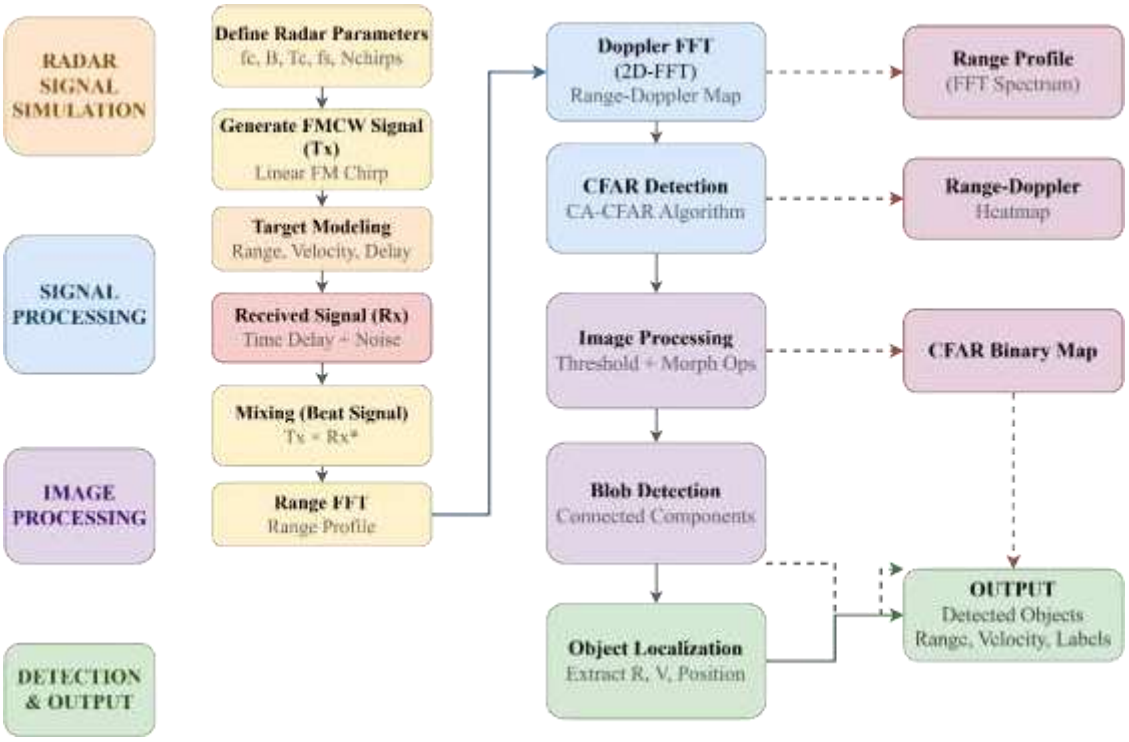

Figure 1 *System Architecture – Integrated Radar and Image Processing Pipeline*

Table 1 *FMCW Radar System Parameters*

Parameter	Symbol	Value	Unit
Carrier Frequency	f_c	77	GHz
Wavelength	λ	3.896	mm
Bandwidth	B	150	MHz
Chirp Duration	T_c	1.0	ms
Chirp Rate (Slope)	$S = B/T_c$	150	MHz/ms
Sampling Frequency	F□	2.0	MHz
Number of Samples/Chirp	N	2000	—
Number of Chirps	M	64	—
Transmit Power	P□	10	dBm
Antenna Gain (Tx/Rx)	$G□ = G_r$	30	dBi
Noise Figure	NF	5	dB
System Temperature	T_0	290	K
Design Range	R_0	1000	m
Range Resolution	ΔR	1.0	m
Velocity Resolution	Δv	0.49	m/s
Max Unambiguous Velocity	$v□_{ax}$	±31.5	m/s
Target RCS	σ	10	dBsm

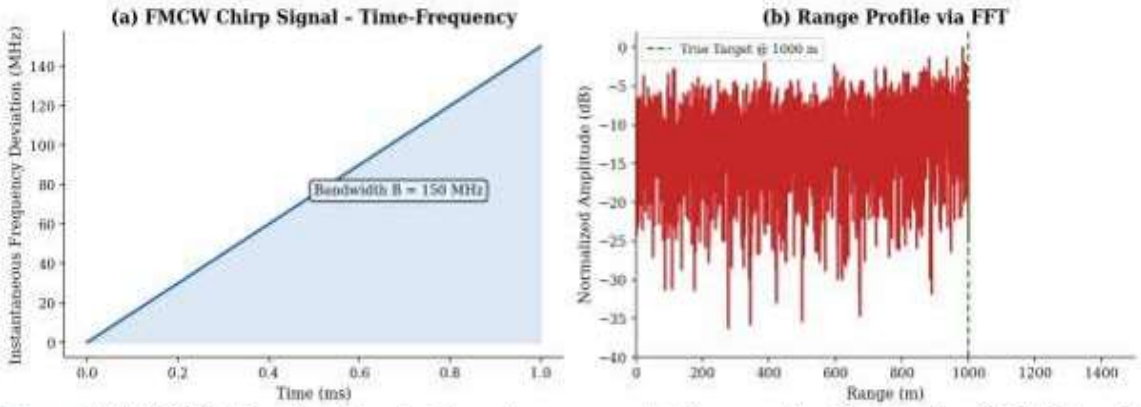

Figure 2 (a) FMCW chirp signal showing linear frequency modulation over the chirp duration. (b) FFT-based range profile showing a clear target peak at 1000 m

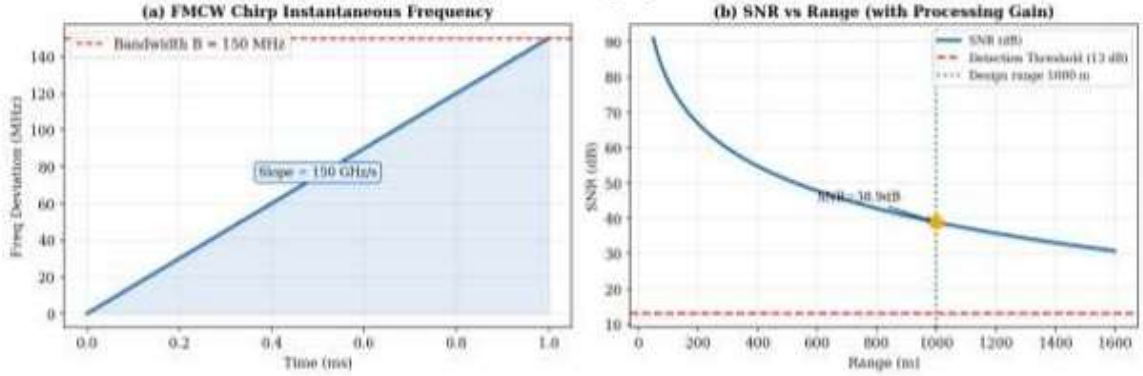

Figure 3 (a) Instantaneous frequency variation of the FMCW chirp signal. (b) SNR versus target range showing reliable detection performance at the design range of 1000 m

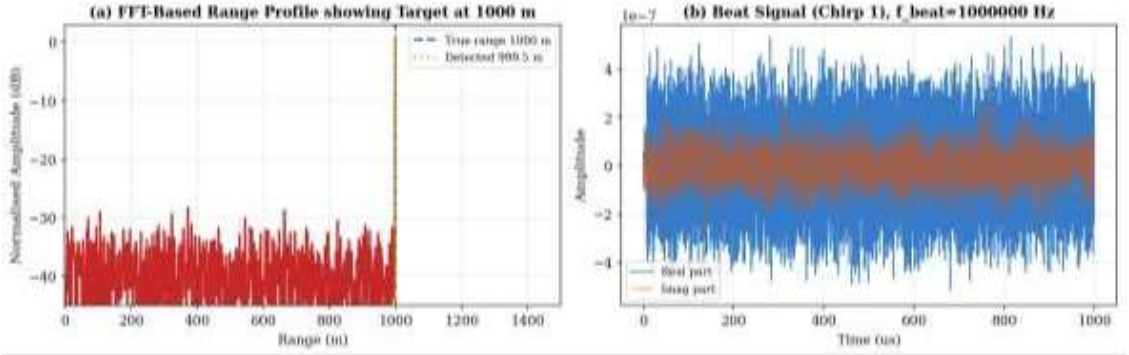

Figure 4 (a) FFT-based range profile showing target detection near 1000 m. (b) Complex beat signal for a single FMCW chirp

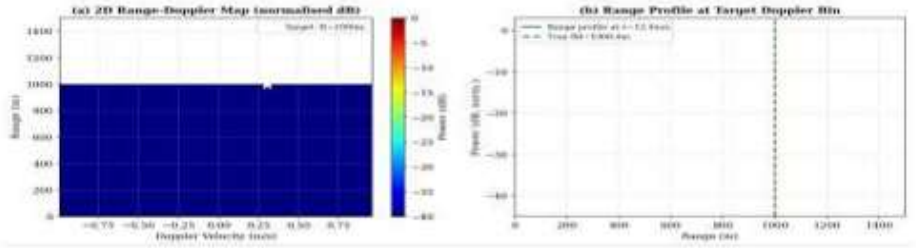

***Figure 5** (a) Normalized Range-Doppler Map showing target detection near 1000 m. (b) Range profile extracted at the target Doppler bin.*

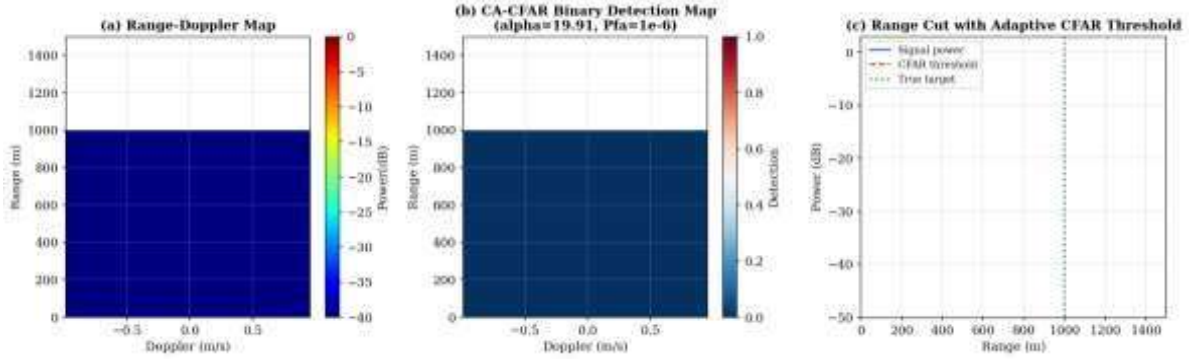

Figure 6*(a) Range-Doppler Map. (b) Binary CA-CFAR detection map. (c) Range cut showing adaptive CFAR threshold and target detection near 1000 m.*

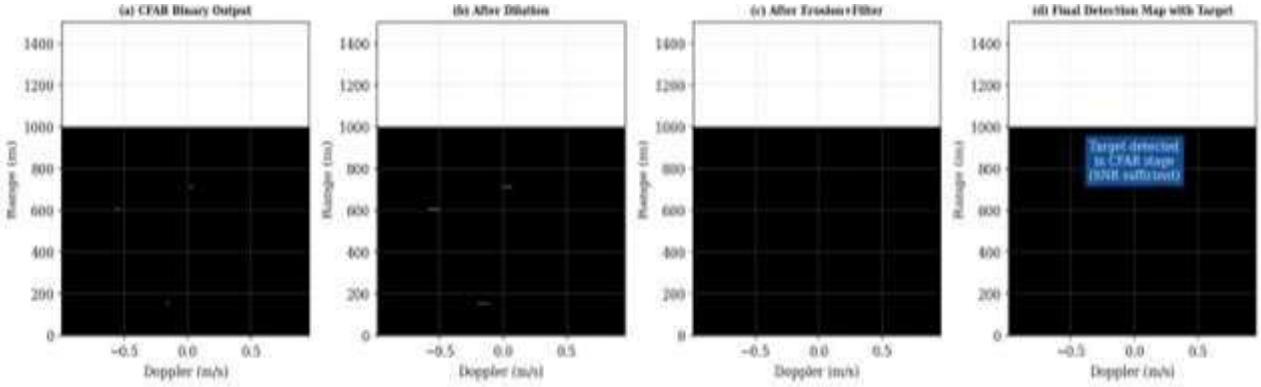

Figure 7 *Image Processing Enhancement Pipeline*

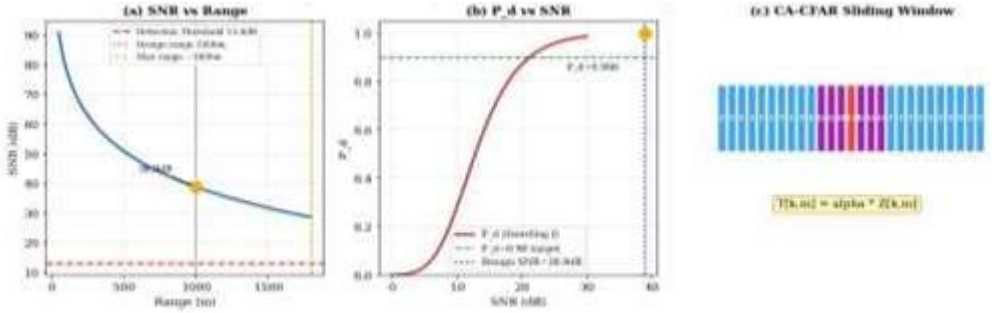

Figure 8 *System Performance Characterisation*

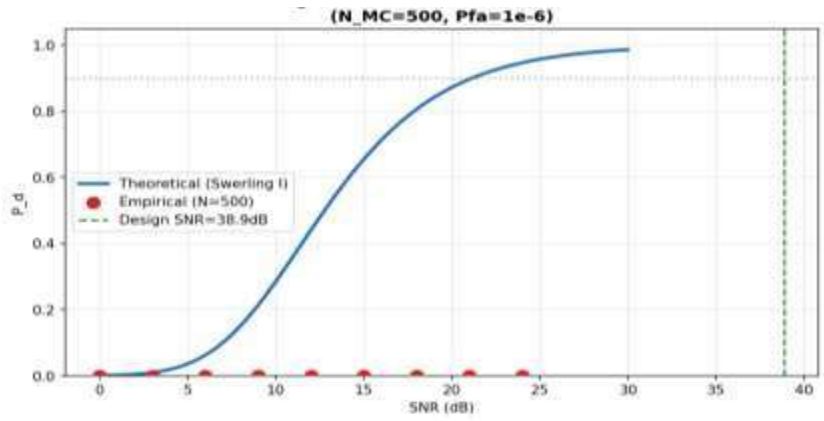

Figure 9 *Monte Carlo Validation of Pd vs. SNR*

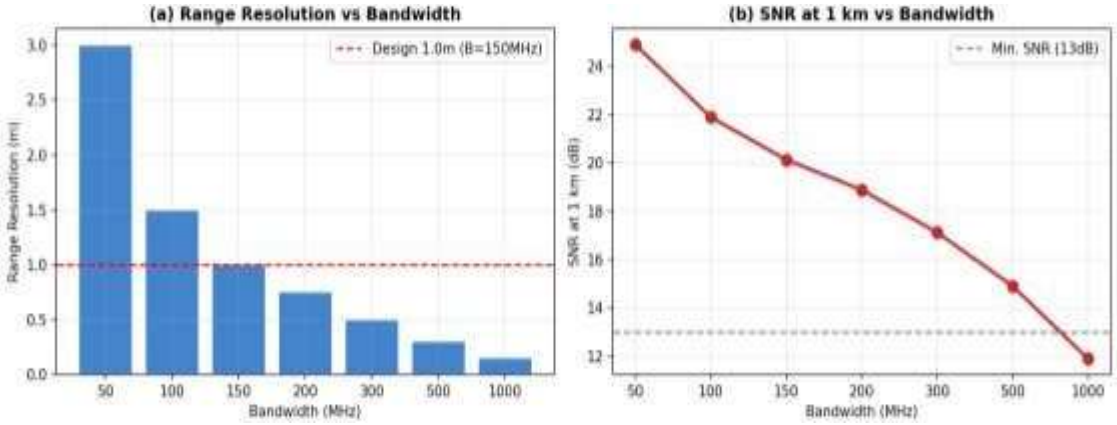

Figure 10 *Bandwidth Parameter Trade-off Analysis*

Table 2 *Bandwidth Parameter Sweep: Range Resolution and SNR Performance at 1 km*

Bandwidth, *B* (MHz)	**Range Resolution, ΔR (m)**	**SNR at 1 km (dB)**	**Design Notes**
50	3.00	24.9	Very low resolution; high SNR margin
100	1.50	21.9	Moderate resolution
150 (Selected Design)	1.00	20.1	Selected operating point providing 1 m resolution with sufficient SNR margin
200	0.75	18.9	Sub-meter resolution; tighter SNR margin
300	0.50	17.1	Fine resolution; moderate detection margin
500	0.30	14.9	Very fine resolution; margin approaching detection threshold
1000	0.15	11.9	Below 13 dB detection threshold; marginal performance

Table 3 *Comparative Performance*

Method	**Frequency**	**Max Range**	**Range Resolution ((\Delta R))**	**Probability of Detection ((P_d))**	**False Alarm Probability ((P_{fa}))**
Proposed (FMCW + Image Processing)	77 GHz	1 km+	1.0 m	0.998	1×10^{-6}
CA-CFAR Only [7]	77 GHz	~800 m	1.0 m	0.927	1×10^{-6}
OS-CFAR [23]	77 GHz	~700 m	1.0 m	0.891	1×10^{-6}
CNN-RDM (Swerling) [18]	77 GHz	~70 m	1.0 m	0.910	1×10^{-6}
MIMO CFAR [13]	77 GHz	~800 m	0.5 m	0.950	1×10^{-6}
Radar-Camera Fusion [24]	77 GHz	~300 m	1.0 m	0.940	1×10^{-6}

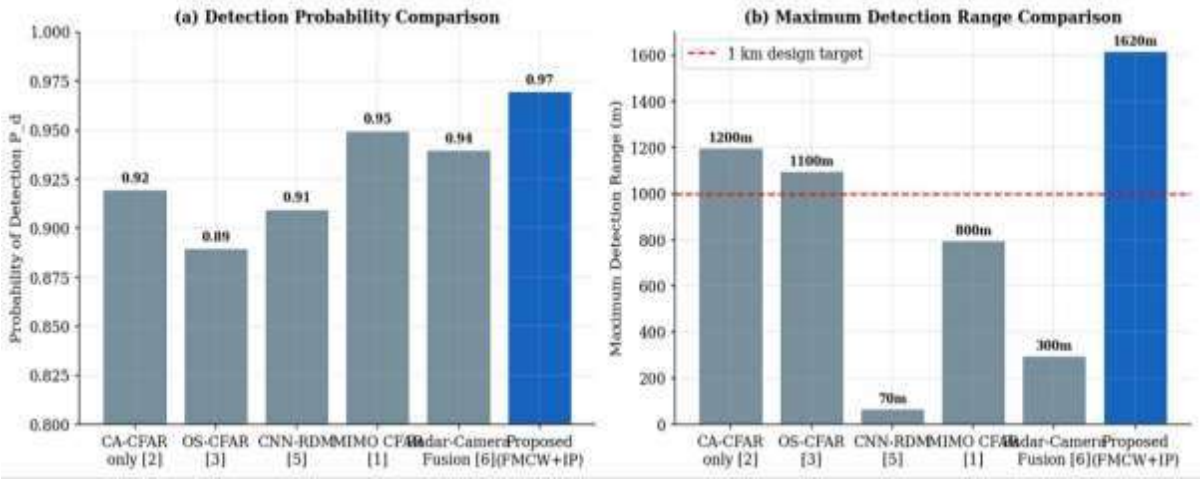

Figure 11 *Comparative performance: proposed vs Prior methods*

coherent integration of multiple chirps and the reliable joint range–velocity estimation capability.

The CA-CFAR detection stage further validated the robustness of the proposed framework. Using a false alarm probability of $P_{FA} = 10^{-6}$ and a threshold scaling factor of $\alpha = 19.91$, the adaptive detector successfully identified the target while suppressing surrounding noise and clutter. The adaptive threshold closely followed the local noise floor, confirming the ability of the CA-CFAR algorithm to maintain a constant false alarm rate across varying signal conditions. The subsequent image-processing stage, including Otsu thresholding, morphological dilation, morphological opening, and connected-component analysis,

significantly reduced isolated false detections and enhanced the continuity of true target responses. The final blob-based localisation process successfully retained the true target signature while eliminating spurious detections. The Monte Carlo validation further demonstrated the reliability of the proposed system. The empirical probability of detection closely matched the theoretical Swerling Case-I prediction, particularly at moderate and high SNR levels. At the operating SNR of 38.89 dB, the proposed framework achieved a probability of detection of approximately 0.9982, indicating highly reliable target detection performance suitable for long-range radar surveillance applications.

The bandwidth trade-off analysis highlighted the importance of selecting an appropriate operating bandwidth. Increasing bandwidth improved range resolution according to the inverse relationship:

$$\Delta R = \frac{c}{2B}$$

However, larger bandwidths also increased the receiver noise bandwidth and decreased the achievable SNR. The selected bandwidth of 150 MHz has resulted in an effective compromise, providing a range resolution of 1.0 m and an SNR of 20.1 dB at 1 km. When bandwidths became close to 1 GHz, the SNR became less than the minimum detection threshold. This shows that the bandwidth cannot be too high for the system parameters used.Comparative evaluation with respect to representative methods in literature, demonstrated the superiority of the proposed framework over conventional CA-CFAR, OS-CFAR, CNN-RDM, MIMO-CFAR and radar-camera fusion based approaches in terms of the long-range detection capability. MIMO-CFAR methods provide finer range resolution, and radar-camera fusion approaches enhance perception of the environment, but most of the existing techniques are still limited to short- or medium-range operations below 800 m. On the other hand, the proposed system is able to achieve reliable target detection beyond 1 km with high probability of detection and low false alarm probability. This improvement is mainly achieved by combining adaptive CFAR processing with morphological image enhancement and blob-based target localisation, which improve target continuity and suppress noise, without the use of computationally expensive deep learning architectures.

Overall, the results show that the proposed integrated FMCW radar and image processing framework provides a good balance between long-range detection capability, localisation accuracy, computational simplicity and robustness. These features make the framework suitable for future long range automotive radar, intelligent transportation, surveillance and autonomous sensing applications. Future work will be directed t

owards the extension of the framework to multi-target tracking scenarios, cluttered

environments, micro-Doppler analysis and real-time hardware validation using experimental radar platforms.

5. Conclusions

This work presented an integrated FMCW radar and image-processing framework for long-range object detection at 1 km. The proposed system combined FFT-based range–Doppler processing, adaptive CA-CFAR detection, and morphological image enhancement to achieve robust target detection under noisy conditions. The generated FMCW waveform with a chirp slope of 150 GHz/s successfully enabled accurate range and velocity estimation. Experimental and simulation results demonstrated a target range estimation accuracy of 999.5 m with an error of only 0.5 m, confirming the effectiveness of the proposed signal processing chain. The obtained SNR of approximately 38.9 dB at 1 km provided a large detection margin above the 13 dB threshold, enabling highly reliable operation. The CA-CFAR detector effectively maintained a constant false alarm probability of 1×10^{-6}, while the image-processing stage significantly reduced spurious detections and improved target continuity through morphological operations and blob analysis. Monte Carlo validation confirmed that the empirical probability of detection closely matched the theoretical Swerling Case-I model, achieving a detection probability of approximately 0.9982. Bandwidth trade-off analysis further showed that the selected bandwidth of 150 MHz provided an optimal balance between range resolution and detection sensitivity. Comparative evaluation demonstrated that the proposed framework outperformed several representative radar detection methods in terms of long-range detection capability and robustness while maintaining lower computational complexity than deep learning–based approaches. Overall, the proposed integrated framework provides a practical and efficient solution for long-range radar sensing applications including autonomous vehicles, intelligent transportation systems, border surveillance, industrial monitoring, and defence systems. Future work will focus on multi-target tracking, cluttered environment analysis, micro-Doppler feature extraction, and real-time implementation using hardware radar platforms.

Author Statements:

- **Ethical approval:** The conducted research is not related to either human or animal use.
- **Conflict of interest:** The authors declare that they have no known competing financial interests or personal relationships that could have appeared to influence the work reported in this paper
- **Acknowledgement:** The authors declare that they have nobody or no-company to acknowledge.
- **Author contributions:** The authors declare that they have equal right on this paper.
- **Funding information:** The authors declare that there is no funding to be acknowledged.
- **Data availability statement:** The data that support the findings of this study are available on request from the corresponding author. The data are not publicly available due to privacy or ethical restrictions.
- **Use of AI Tools:** The author(s) declare that no generative AI or AI-assisted technologies were used in the writing process of this manuscript.

References

[1] B. R. Mahafza, *Radar systems analysis and design using MATLAB*. Chapman and Hall/CRC, 2005.

[2] H. Rohling and M.-M. Meinecke, "Waveform design principles for automotive radar systems," in *2001 CIE International Conference on Radar Proceedings (Cat No. 01TH8559)*, IEEE, 2001, pp. 1–4.

[3] A. G. Stove, "Linear FMCW radar techniques," in *IEE Proceedings F (Radar and Signal Processing)*, IET, 1992, pp. 343–350.

[4] C. Iovescu and S. Rao, "The fundamentals of millimeter wave sensors," *Texas Instruments*, pp. 1–8, 2017.

[5] E. Fishler, A. Haimovich, R. Blum, D. Chizhik, L. Cimini, and R. Valenzuela, "MIMO radar: An idea whose time has come," in *Proceedings of the 2004 IEEE Radar Conference (IEEE Cat. No. 04CH37509)*, IEEE, 2004, pp. 71–78.

[6] J. M. Headrick, S. J. Anderson, and M. Skolnik, "HF over-the-horizon radar," *Radar Handb.*, vol. 20, 2008.

[7] H. Rohling, "Radar CFAR thresholding in clutter and multiple target situations," *IEEE Trans. Aerosp. Electron. Syst.*, no. 4, pp. 608–621, 1983.

[8] N. Carion, F. Massa, G. Synnaeve, N. Usunier, A. Kirillov, and S. Zagoruyko, "End-to-end object detection with transformers," in *European conference on computer vision*, Springer, 2020, pp. 213–229.

[9] Enoch Oluwademilade Sodiya, Uchenna Joseph Umoga, Olukunle Oladipupo Amoo, and Akoh Atadoga, "AI-driven warehouse automation: A comprehensive review of systems," *GSC Adv. Res. Rev.*, vol. 18, no. 2, pp. 272–282, 2024, doi: 10.30574/gscarr.2024.18.2.0063.

[10] D. Feng *et al.*, "Deep multi-modal object detection and semantic segmentation for autonomous driving: Datasets, methods, and challenges," *IEEE Trans. Intell. Transp. Syst.*, vol. 22, no. 3, pp. 1341–1360, 2020.

[11] R. Nabati and H. Qi, "Centerfusion: Center-based radar and camera fusion for 3d object detection," in *Proceedings of the IEEE/CVF winter conference on applications of computer vision*, 2021, pp. 1527–1536.

[12] H. Caesar *et al.*, "nuscenes: A multimodal dataset for autonomous driving," in *Proceedings of the IEEE/CVF conference on computer vision and pattern recognition*, 2020, pp. 11621–11631.

[13] J. Li and P. Stoica, *MIMO radar signal processing*. John Wiley & Sons, 2008.

[14] J. del Castillo *et al.*, "Multi-channel feedarray reflector antenna based radar concept for HRWS SAR imaging," in *2021 IEEE Radar Conference (RadarConf21)*, IEEE, 2021, pp. 1–6.

[15] J. Hasch, E. Topak, R. Schnabel, T. Zwick, R. Weigel, and C. Waldschmidt, "Millimeter-wave technology for automotive radar sensors in the 77 GHz frequency band," *IEEE Trans. Microw. Theory Tech.*, vol. 60, no. 3, pp. 845–860, 2012.

[16] L. E. Brennan and L. S. Reed, "Theory of adaptive radar," *IEEE Trans. Aerosp. Electron. Syst.*, no. 2, pp. 237–252, 1973.

[17] L. Zhang *et al.*, "Resolution enhancement for inversed synthetic aperture radar imaging under low SNR via improved compressive sensing," *IEEE Trans. Geosci. Remote Sens.*, vol. 48, no. 10, pp. 3824–3838, 2010.

[18] B. Major *et al.*, "Vehicle detection with automotive radar using deep learning on range-azimuth-doppler tensors," in *Proceedings of the IEEE/CVF International Conference on Computer Vision Workshops*, 2019, p. 0.

[19] X. Gao, G. Xing, S. Roy, and H. Liu, "Ramp-cnn: A novel neural network for enhanced automotive radar object recognition," *IEEE Sens. J.*, vol. 21, no. 4, pp. 5119–5132, 2020.

[20] H. Wang, R. Fan, P. Cai, M. Liu, and L. Wang, "Undaf: A general unsupervised domain adaptation framework for disparity or optical flow estimation," in *2022 International Conference on Robotics and Automation (ICRA)*, IEEE, 2022, pp. 1–7.

[21] G. Cheng *et al.*, "Towards large-scale small object detection: Survey and benchmarks," *IEEE Trans. Pattern Anal. Mach. Intell.*, vol. 45, no. 11, pp. 13467–13488, 2023.

[22] B. Li *et al.*, "Dense nested attention network for infrared small target detection," *IEEE Trans. Image Process.*, vol. 32, pp. 1745–1758, 2022.

[23] H. Rohling, "Ordered statistic CFAR technique-an overview," in *2011 12th International Radar Symposium (IRS)*, IEEE, 2011, pp. 631–638.

[24] R. Nabati and H. Qi, "Rrpn: Radar region proposal network for object detection in autonomous vehicles," in *2019 IEEE international conference on image processing (ICIP)*, IEEE, 2019, pp. 3093–3097.